SCIENCE CHINA
Technological Sciences

• Article •

October 2014 Vol.57 No.10: 2037–2043
doi: 10.1007/s11431-014-5664-4

# Study on the critical diameter of the subway tunnel based on the pressure variation

SUN ZhenXu[1*], YANG GuoWei[1] & ZHU Lan[2]

[1] *Key Laboratory for Mechanics in Fluid Solid Coupling Systems, Institute of Mechanics, Chinese Academy of Sciences, Beijing 100190, China;*
[2] *Beijing Rail and Transit Design & Research Institute CO., LTD, Beijing 100089, China*

Received January 2, 2014; accepted June 9, 2014; published online September 11, 2014

When the subway train operates at a speed higher than 100 km/h, the corresponding aerodynamic issue becomes severe. To meet the future requirement for the speedup of subway trains, a research on the critical diameters of the subway tunnel for trains operating at 120 and 140 km/h has been performed based on passengers' aural discomfort caused by rail tunnel pressure variation. A three-dimensional computational fluid dynamic approach has been adopted for analysis. Meanwhile, trains with different airtight indices are considered and the pressure variations inside and outside the trains are both under investigation. Based on the corresponding criteria for different airtight indices, critical tunnel diameters for trains running at different speeds have been determined. This study would aid in the tunnel section design for future high-speed subway trains.

**tunnel pressure waves, airtight index, aural discomfort, blockage ratio**

**Citation:** Sun Z X, Yang G W, Zhu L. Study on the critical diameter of the subway tunnel based on the pressure variation. Sci China Tech Sci, 2014, 57: 2037–2043, doi: 10.1007/s11431-014-5664-4

## 1 Introduction

As the speedup of the urbanization, the cutting-edge industries in every megacity further gather into the center of the city, while the citizens generally reside outside. The cities expand dramatically, especially the population and the land of the city, resulting in urgent requirement for the commute for the downtown and the suburb. As a result, the distance of the commute expands and the efficiency to commute in such a long distance decreases. Currently, the development of urban transport becomes a limitation. The normal running speed of the subway trains in China is around 80 km/h, which is far from the high-speed requirement. Consequently, developing subway trains with higher speeds becomes the most urgent need in the current circumstance.

However, as the velocity of subway trains increases, a series of aerodynamic problems emerge. The running drag increases dramatically, which brings the energy-consuming issues. The magnitude of the tunnel pressure waves increases too, and the noise circumstance deteriorates rapidly due to the increase in aerodynamic noise. The above phenomena also bring a series of engineering problems. The microwaves induced by the initial compression waves will cause aeroacoustic problems in the surroundings and do fatigue damage to the surrounding buildings. When the pressure waves propagate inside the train, aural discomfort for the passengers may arise. The pressure waves may also do damage to the structures of the train and facilities in the tunnel.

The approaches for metro gauges introduced in the "Standard of metro gauges" used currently are only applicable for a maximum speed of 100 km/h. However, for the

*Corresponding author (email: sunzhenxu@imech.ac.cn)

speed higher than 100 km/h, there are no direct ways. At the same time, a few literatures could be referred to on aerodynamic study for high-speed subway trains. As a result, it is meaningful to perform the research on aural discomfort and metro gauge for subway trains at high speeds, both in the academic aspect and in the engineering aspect.

The study on tunnel aerodynamics can be classified into four groups, namely the theoretical analysis [1,2], the real vehicle tests [3,4], the moving model rig tests [5,6], and numerical simulations. Relatively speaking, numerical simulations benefit from low cost, short designing period, and easy investigation on scenes in extreme conditions, which could strongly support the engineering application. For the numerical approaches, three types could be summarized, which are one-dimensional approaches [6,7], two-dimensional approaches [8,9], and three-dimensional approaches [6,7], respectively. The flow details for trains passing by the tunnel or passing by each other in the tunnel could be precisely simulated by three-dimensional approaches [10], such as the flow around the train and the aerodynamic loads on the train, which will aid in the structural design of the train.

In the present paper, the three-dimensional numerical approach has been adopted and analysis of tunnel pressure waves outside and inside the train has been performed with different airtight characteristics, different running speeds, and different tunnel cross-sections. The characteristics of pressure waves under the above conditions have been provided. An assessment of passengers' aural discomfort has been conducted comparing corresponding pressure criteria for different airtight indices. Finally, the critical tunnel diameters for trains under different speeds are obtained.

## 2 Computational models and conditions

### 2.1 The train model

The S-type subway train is taken as the computational model in the present paper, whose cross-sectional area is 10.49 $m^2$. This train is modified from the original A-type subway train to meet the future speedup requirement. Compared with the A-type train, a streamlined head could be observed from the S-type train which is about 3 m in length. Meanwhile, the cross section of the S-type train is the same as the prototype. Figure 1 shows the streamlined head of the S-type train.

Hybrid mesh is adopted for the mesh generation in the moving zone. The core area around the train uses unstructured grids, while the region near the wall uses prism grids to capture the flow details within the boundary layer. The $y+$ along the surface of the train ranges from 30 to 100 to ensure the use of wall functions. Meanwhile, structured grids are generated outside the core region for mesh updation. The total number of grids is around 5.6 million.

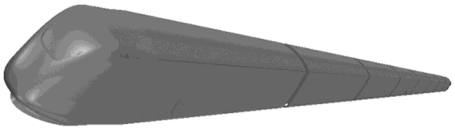

**Figure 1** The streamlined head of the S-type train.

### 2.2 The tunnel model

The different intensities of tunnel pressure waves are generated in tunnels at different lengths. However, the magnitude of the pressure waves is not proportional to the length of the tunnel. Based on the condition that the maximum positive pressure emerges on top of the leading streamline, the worst tunnel length could be determined, which takes the form as

$$L_{\text{tunnel}} = L_{\text{train}}\left(\frac{1}{2M}+\frac{1}{1-M}\right),$$

where $M$ is the Mach number of the train and $L_{\text{train}}$ is the length of the train. Taking 8-grouping subway trains into consideration, the length of the train is around 200 m. Assuming that the running speed of the train is 120 km/h, the worst tunnel length could be obtained as 1200 m according to the above formula. The train experiences a worst pressure condition in this case. The cross section of the tunnel is shown in Figure 2.

Taking $D$ as the width of the high-speed train, the lengths of the domain before and after the tunnel are both set as 90.3$D$, the width of the domain is set as 30.1$D$, and the length of the tunnel is $L_{\text{TU}}$=401.2$D$. The whole domain for the train passing by the tunnel is shown in Figure 3.

### 2.3 Boundary conditions

At present, the maximum running speed of subway trains in the underground tunnel has already reached up to 120 km/h for the Guangzhou Metro Line 3, as well as the under-construction metro lines in Shenzhen and Shanghai. Meanwhile, for the New Airport Line and R1 Line in Beijing, 120

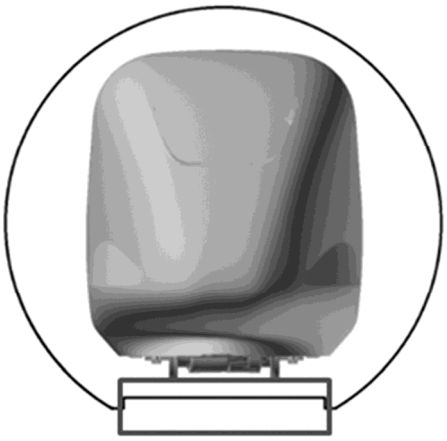

**Figure 2** The cross section of the tunnel.

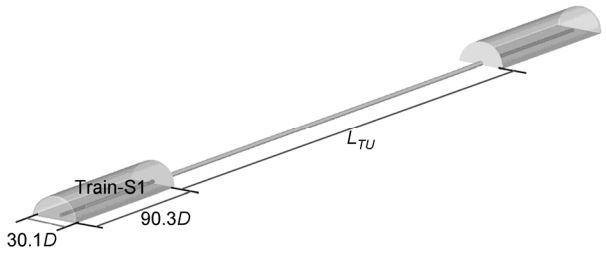


**Figure 3** The computational domain for the train passing by the tunnel.

km/h is the suggested speed for the train running in the tunnel. As a result, the basic running speed considered in the present paper is set as 120 km/h. To face the future requirement for much higher speed, 140 km/h is also taken into consideration. The critical tunnel diameters for speeds above are under investigation.

The moving mesh technique is adopted in the present paper. Consequently, the ground and the tunnels are set as stationary no-slip walls while the train is moving at the real running speed. The pressure outlet boundary is imposed with 1 atm for the outer space.

### 2.4 Configuration of pressure probes

Three probes are placed in the streamlined head of the leading car, top of the middle car, and the streamlined head of the trailing car, respectively. As a representative of each car, the pressure variations of these probes during the train passing by the tunnel are recorded to represent the pressure characteristics of each car. The exact configuration of the probes is shown in Figure 4.

## 3 Algorithms

### 3.1 Algorithms for the analysis of pressure waves outside the train

The analysis of pressure waves outside the train should be first performed. The unsteady Reynolds-Averaged Navier-Stokes approach has been adopted to solve the flow field when the train passes by the tunnel. The fluctuating values lead to the emergence of Reynolds stress terms in the Reynolds-averaged equations. Therefore, a turbulence model needs to be introduced to close the equations to solve each physical quantity in the flow field. The primary transport variables are governed by conservation equations of mass and momentum:

$$\frac{\partial \rho}{\partial t}+\nabla\cdot(\rho \boldsymbol{v})=0,$$


**Figure 4** Configuration of pressure probes on the train.

$$\frac{\partial}{\partial t}(\rho \boldsymbol{v})+\nabla\cdot(\rho \boldsymbol{v}\boldsymbol{v})=-\nabla p+\nabla\cdot(\mu\nabla \boldsymbol{v})+\boldsymbol{S}_{\boldsymbol{M}},$$

where $\boldsymbol{S}_{\boldsymbol{M}}$ is the source term, which could be expressed as

$$\boldsymbol{S}_{\boldsymbol{M}}=\rho \boldsymbol{g}+\frac{\partial}{\partial x_i}\left(\mu\frac{\partial v_i}{\partial x_j}\right)\boldsymbol{e}_j-\frac{2}{3}\nabla\left(\mu\nabla\cdot \boldsymbol{v}\right).$$

The fluctuating values lead to the emergence of Reynolds stress terms in the Reynolds-averaged equations. The turbulence model needs to be introduced to close the equations to solve each physical quantity in the flow field.

The RNG $k$–$\varepsilon$ turbulence model is adopted [11], which evolves on the basis of the standard $k$–$\varepsilon$ model and satisfies the Reynolds stress constraints. This model includes the effect of swirl on turbulence, which enhances the accuracy for swirling flows. Besides, this model is a two-equation model that is obtained from adding the transport equations with turbulent kinetic energy $k$ and turbulent dissipation rate $\varepsilon$, which are

$$\frac{\partial}{\partial t}(\rho k)+\frac{\partial}{\partial x_j}(\rho k v_j)=\frac{\partial}{\partial x_j}\left[\left(\mu+\frac{\mu_t}{\sigma_k}\right)\frac{\partial k}{\partial x_j}\right]+G_k+G_b-\rho\varepsilon-Y_M,$$

$$\frac{\partial}{\partial t}(\rho \varepsilon)+\frac{\partial}{\partial x_j}(\rho \varepsilon v_j)=\frac{\partial}{\partial x_j}\left[\left(\mu+\frac{\mu_t}{\sigma_\varepsilon}\right)\frac{\partial \varepsilon}{\partial x_j}\right]+\rho C_1 S\varepsilon-\rho C_2\frac{\varepsilon^2}{k+\sqrt{\nu\varepsilon}}+C_{1\varepsilon}\frac{\varepsilon}{k}C_{3\varepsilon}G_b.$$

The expressions of the variables in the above equations could be referred to in the literature [11], which will not be listed in the present paper for simplicity. When solving the above equations, the SIMPLE algorithm has been adopted to deal with the pressure-velocity coupling problem, while the second-order upwind discretization has been used for the momentum, $k$, and $\varepsilon$ equations.

The relative motion between trains needs to be considered in the present paper. Traditional computational fluid dynamics (CFD) methods assume that the reference coordinate system is placed on the train body and uniform flow is imposed on the inlet of the computing domain, which is unavailable in the present paper. Taking into account the characteristics of the running trains, the sliding mesh should be adopted [12], and the dynamic layering method is used in the running direction of the train.

The dynamic layering method could be used to add or remove layers of cells adjacent to a moving boundary based on the height of the layer adjacent to the moving surface.

As shown in Figure 5, if the boundary is moving upward, the cells in the $j$th layer will be compressed until $h<\alpha_c h_{\text{ideal}}$, where $\alpha_c$ ($0<\alpha_c<1$) is the combined coefficient and $h_{\text{ideal}}$ is the ideal cell height. Then, the cells in the $j$th and $i$th layer will be combined together; if the boundary is moving down-

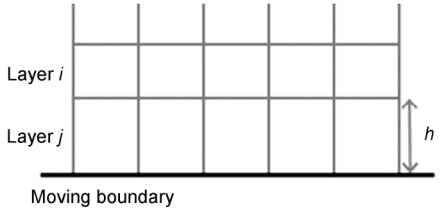


**Figure 5** Schematic of the dynamic layering method.

ward, the cell heights are allowed to increase until $h<(1+\alpha_s)h_{\text{ideal}}$, where $\alpha_s$ ($0<\alpha_s<1$) is the splitting coefficient. When this condition is met, the cells are split based on the specified layering option: Constant height or constant ratio.

### 3.2 Algorithms for the analysis of pressure waves inside the train

After obtaining the pressure variations outside the train, an uncoupled approach could be adopted to solve the pressure variations inside the train, which takes the form as [13]

$$p_i = p_0\left(1-\mathrm{e}^{-\frac{t}{\tau}}\right),$$

where $p_i$ is the pressure variation inside the train between adjacent time steps, $p_0$ is the difference between the pressure outside the train and the pressure inside the train in the current time step, $t$ is the time step, $\tau$ is the airtight index, taking the unit as $s$. The pressure variation inside the train could be obtained via the above formula on the condition that the pressure variations outside the train and the airtight index of the train are both known.

### 3.3 Airtight index

When subway trains pass by the tunnel, the pressure waves could propagate into the inside of the train according to the airtight characteristics of the trains. The quality of airtightness of the train could directly influence the characteristics of pressure waves inside the train. Better quality of airtightness of the train corresponds to a smaller airtight index, and vice versa. Table 1 shows the range of airtight index of the train with different quality of airtightness.

However, the airtight index of the high-speed subway train is uncertain at present. As a result, two kinds of airtight indices are taken into consideration. One is referred to as unsealed trains, the airtight index of which is 0.7 s; the other is referred to as ordinary quality of subway trains, the airtight index is 5 s. The former airtight index is mainly discussed during the analysis, since most of the subway trains in China belong to this type.

**Table 1** The range of airtight index of the train with different quality of airtightness

| Airtightness assessment | Airtight index | Type of the train |
|---|---|---|
| Unsealed | $\tau<1$ s | |
| Ordinary | 1 s$<\tau<$6 s | Eurocity |
| Good | 6 s$<\tau<$10 s | ICE1, TGV |
| Excellent | $\tau>10$ s | ICE3, Transrapid |

### 3.4 Criteria of aural discomfort

After obtaining the pressure waves inside the train, the evaluation of aural discomfort should be performed. As a result, the criterion of aural discomfort should be provided in advance. A series of criteria exist, of which the American Standard is mostly accepted and widely used in Guozhou Metro Line 3 and Hong Kong New Airport Line. American Standard mainly deals with the unsealed train and can be expressed as follows: The pressure variation ratio should be less than 410 Pa/s. For sealed vehicles, 800 Pa/3 s is taken as the evaluation criterion according to the literature released by the authorities.

## 4 Results and discussion

To determine the critical tunnel diameter for specific running speed, a series of tunnel diameters should be considered and the pressure histories in each diameter should be obtained so as to compare with the specific criterion. Consequently, a large amount of computational cost should be taken. In the present paper, the discussion is only focused on the case that the tunnel diameter basically meets the criterion of aural discomfort. First, the numerical validation for CFD analysis has been performed.

### 4.1 Numerical validation

In this section the experiments in literature [14] are taken as the test case for numerical validation. The experiments were conducted at the von Karman Institute for Fluid Dynamics. The tunnel is 6 meter long with a uniform circular cylindrical section of 99 mm in diameter. The long train model which is 600 mm in length and 38 mm in diameter is adopted for validation. It has a conical nose with an angle of 60° between the axis and the directrix. Numerical models and computational conditions keep the same with the experimental ones. The running speed of the train is chosen as 140 km/h. An axisymmetrical computation has been performed with the same algorithms proposed in the present paper. A typical pressure pattern is obtained for the probe at $l$=900 mm from the tunnel extrance, which is shown in Figure 6 together with the experimental results.

As seen above, the numerical results agree well with the experimental results, indicating that the algorithms proposed in the present paper could be used for further study.

### 4.2 Critical tunnel diameter for the speed of 120 km/h

When the subway train runs at 120 km/h, the tunnel diame-

ter of 6.0 m is chosen for discussion. The blockage ratio in this case is about 0.4. The pressure histories of three probes outside the train and inside the train under two airtight indices are shown in Figures 7–9.

As seen above, the three stages could be divided from the pressure histories, which are entering the tunnel, running in the tunnel, and leaving the tunnel, respectively, just as shown in the rectangular boxes. As shown in Figure 7, when the train runs into the tunnel, the air around the train is compressed by the tunnel wall and the pressure increases dramatically, forming the initial compressible pressure wave. As the train moves forward, the length of the annulus space between the train and the tunnel increases continuously and the pressure in front of the train increases further. Meanwhile, the pressure around the part of the train which has already been in the tunnel grows higher too. As seen in Figure 8, the middle car mainly experiences negative pressure, and the magnitude of the pressure variations is obviously smaller than the leading car. As seen in Figure 9, after the trailing streamline enters the tunnel, an expansion wave is generated at the entrance and propagates along the tunnel. The pressure decreases as long as the expansion wave passes by. Meanwhile, reflection occurs when the pressure waves reach at the portals and pressure forms get exchanged then. For example, compressive waves may change into expansion waves, and vice versa. The pressure around the train varies due to the propagation of pressure waves.

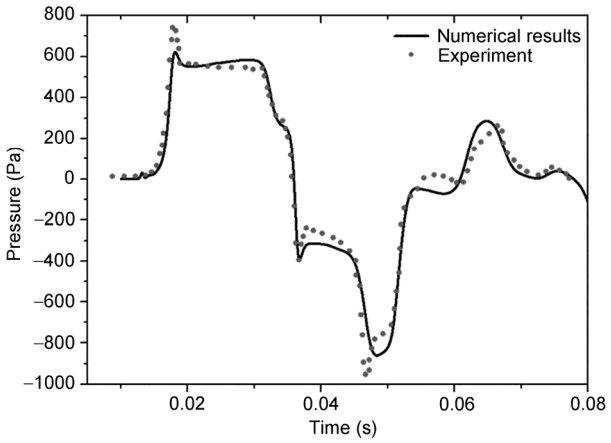


**Figure 6** Comparisons between experimental and numerical data at $l$=900 mm.

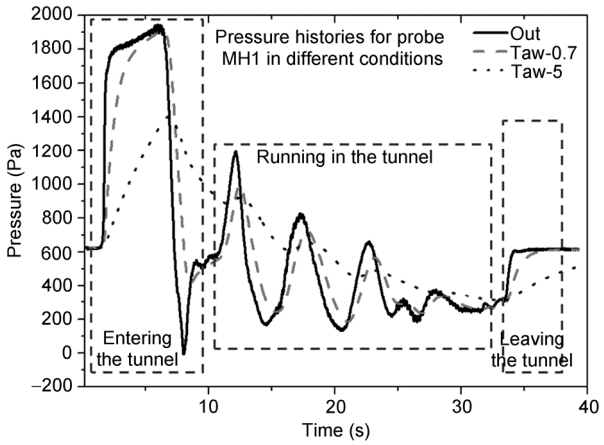


**Figure 7** Pressure histories for probe MH1 in different conditions.

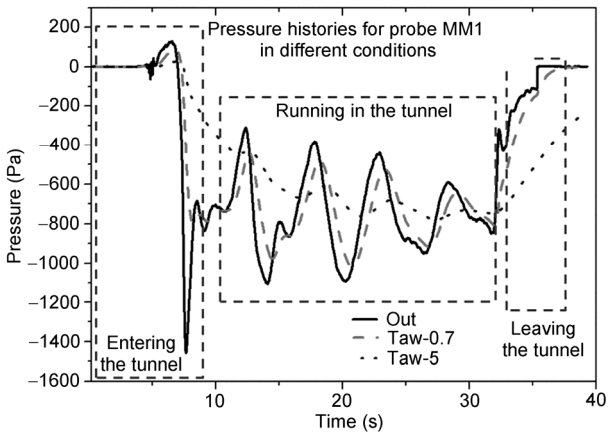


**Figure 8** Pressure histories for probe MM1 in different conditions.

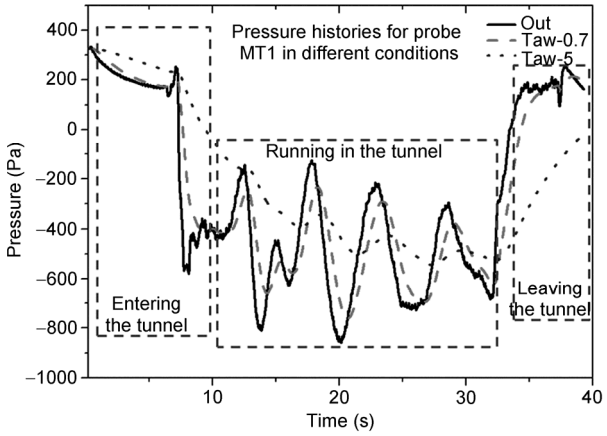


**Figure 9** Pressure histories for probe MT1 in different conditions.

For the probe in the leading streamline, the initial pressure rise comes from the initial compression wave by the interaction between the leading streamline and the tunnel. The first pressure drop comes from the expansion wave that is generated when the trailing streamline enters the tunnel. In long tunnel conditions, a time gap exists between the generation of the initial compression wave and expansion wave, so a steady period could be observed during the pressure drop.

Evident difference of the pressure variations could be found between the trailing streamline and leading streamline. Since the trailing streamline enters the tunnel a little later than the leading streamline, the initial compression wave hardly affects the trailing streamline. As a result, the initial pressure rise could not be detected and the pressure drops directly.

Then, we will focus on the pressure variations inside the train under different airtight indices. It can be seen clearly

that the magnitude of the pressure variation and the variation ratio inside the train are both smaller than those outside the train. The higher the airtight index, the smaller the magnitude and the pressure variation ratio, indicating that the pressure inside the train is much more comfortable.

The maximum pressure variation ratios for the probes when the train enters the tunnel and runs in the tunnel are shown in Tables 2 and 3.

As seen above, the pressure variation ratio is much greater than the corresponding criterion when the train enters the tunnel and much smaller than the corresponding criterion when the train runs in the tunnel. When the train entering the tunnel, if the ratio is taken as the representative to determine the critical tunnel diameter, it will bring expensive engineering cost. It is a waste compared with the case when the train runs in the tunnel. Concerning that long tunnels are frequently encountered, the pressure variation ratio when the train runs in the tunnel is chosen to determine the critical tunnel diameter. As for the high pressure variation ratio generated when the train enters the tunnel, kinds of buffering devices could be supplemented at the tunnel portals. The maximum pressure variation ratio when the train runs in the tunnel is 335 Pa/s, which satisfies the American criterion of aural comfort (410 Pa/s).

To take all the scenes the subway train encounters into consideration, other scenes (such as accelerating and decelerating in the tunnel, passing by the air shaft in the tunnel, and entering the subway station) are all under investigation. The results reveal that of all the scenes only the case that the train passes by the air shaft in the tunnel gets worse situations, of which the pressure variation ratio is slightly higher than the American Standard. However, this also could be relieved by equipping buffering device in the tunnel.

Based on all the above scenes, the critical tunnel diameter is 6 m for the train that runs in the tunnel at a speed of 120 km/h. This diameter could satisfy the criterion of aural discomfort in most scenes and for those scenes that do not comply with the criterion buffering device should be equipped.

### 4.3 Critical tunnel diameter for the speed of 140 km/h

Since the analysis procedure in the present case is the same as the one in the above section, simplified discussion will be performed in this section. A diameter of 7 m is taken into consideration for the speed of 140 km/h and the blockage ratio is 0.33. The pressure histories of three probes outside the train and inside the train under two airtight indices are shown in Figure 10.

**Table 2** The maximum pressure variation ratios for the probes when the train enters the tunnel

| | MH1 | MM1 | MT1 |
|---|---|---|---|
| $\tau$=0.7 s | 639 Pa/s | 622 Pa/s | 325 Pa/s |
| $\tau$=5 s | 193 Pa/s | 139 Pa/s | 120 Pa/s |

**Table 3** The maximum pressure variation ratios for the probes when the train runs in the tunnel

| | MH1 | MM1 | MT1 |
|---|---|---|---|
| $\tau$=0.7 s | 335 Pa/s | 305 Pa/s | 325 Pa/s |
| $\tau$=5 s | 113 Pa/s | 106 Pa/s | 80 Pa/s |

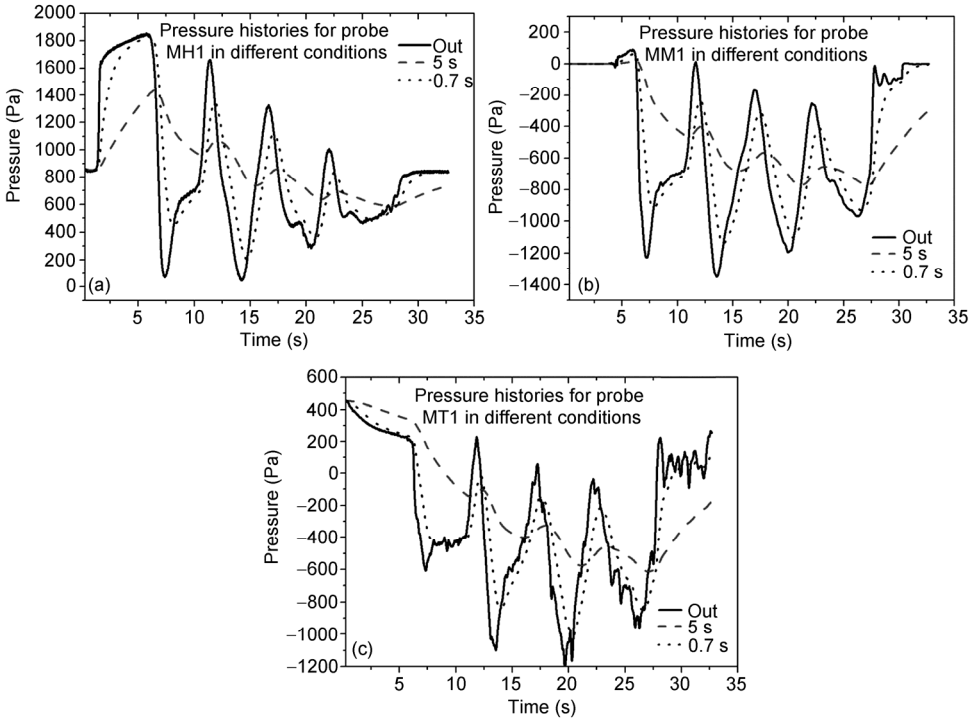


**Figure 10** Pressure histories for the three probes in different conditions. (a) MH1, (b) MM1, (c) MT1.

As seen above, the characteristics of pressure variation are almost the same with the speed of 120 km/h except that the magnitude in the present case is a little bigger. Similarly, the maximum pressure variation ratios for the probes when the train enters the tunnel and runs in the tunnel are shown in Tables 4 and 5.

For the sealed train, the pressure variation ratios of all the probes satisfy the corresponding criterion of aural discomfort. However, for the unsealed train, the maximum pressure variation ratio is 413 Pa/s when the train runs in the tunnel, which is slightly higher than the American Standard. Considering the worst length of the tunnel is used, the maximum pressure variation ratio may be a little higher than the present value, hence buffering device is suggested to be used in the special part of the tunnel. Considering other aspects such as engineering cost, 7 m is determined as the critical tunnel diameter for the running speed of 140 km/h.

## 5 Conclusions

Three-dimensional CFD numerical approach is adopted in the present paper, and the passengers' aural discomfort is discussed for the train passing by the tunnel at a high speed. Based on the corresponding criterion of aural discomfort, the critical tunnel diameters for the speeds of 120 and 140 km/h are determined. The main conclusions are as follows.

1) When the subway train runs at a speed higher than 100 km/h, the aerodynamic characteristics should be taken into consideration, including the running drag, tunnel pressure waves, and aerodynamic noise. The designs of the head of the train and cross section of the tunnel both need to be considered.

2) Big pressure variation emerges when the train enters the tunnel, which will bring aural discomfort problems for the passengers. Therefore, for the running of high-speed subway trains, proper speed deceleration should be performed and certain buffering devices could be equipped at the tunnel portals to relieve the initial pressure rise.

3) 6 m is determined as the critical tunnel diameter for the speed of 120 km/h. This diameter could satisfy the criterion of aural discomfort in most scenes and for those scenes that do not comply with the criterion buffering device should be equipped.

4) 7 m is determined as the critical tunnel diameter for the speed of 140 km/h. This diameter could satisfy the criterion of aural discomfort in most scenes and for those scenes that do not comply with the criterion buffering device should be equipped.

**Table 4** The maximum pressure variation ratios for the probes when the train enters the tunnel

| | MH1 | MM1 | MT1 |
|---|---|---|---|
| $\tau$=0.7 s | 693 Pa/s | 594 Pa/s | 389 Pa/s |
| $\tau$=5 s | 221 Pa/s | 199 Pa/s | 137 Pa/s |

**Table 5** The maximum pressure variation ratios for the probes when the train runs in the tunnel

| | MH1 | MM1 | MT1 |
|---|---|---|---|
| $\tau$=0.7 s | 398 Pa/s | 413 Pa/s | 402 Pa/s |
| $\tau$=5 s | 147 Pa/s | 151 Pa/s | 156 Pa/s |

*This work was supported by the National Basic Research Program of China ("973" Project) (Grant No. 2011CB711100), and the National Natural Science Foundation of China (Grant No. 11302233). Computing Facility for Computational Mechanics Institute of Mechanics, Chinese Academy of Sciences is gratefully acknowledged.*

1 Howe M S. On the infrasound generated when a train enters a tunnel. J Fluid Struct, 2003, 17: 629–642
2 Zhao Y, Gao B, Zhang Z J. Three-dimensional numerical simulation of tunnel pressure waves (in Chinese). Subgrade Eng, 2007, 4: 12–14
3 Raghunathan R S, Kim H D, Setoguchi T. Aerodynamics of high-speed railway train. Prog Aerosp Sci, 2002, 38: 469–514
4 Wan X Y, Wu J. *In-situ* test and study on the aerodynamic effect of the rolling stock passing through tunnels with a speed of 200 km/h (in Chinese). Mod Tunn Technol, 2006, 43: 43–48
5 Baker C J, Dalley S, Johnson J, et al. The slipstream and wake of a high-speed train. P I Mech Eng F-J Rai, 2001, 215: 83–99
6 Zhao W C, Gao B, Wang Y X, et al. Analysis of the pressure wave variation generated by a high-speed train passing through a tunnel (in Chinese). Mod Tunn Technol, 2004, 41: 16–19
7 Thermo Tun-Software[EB/OL]. http://www.thermotun.com/index.htm.
8 Wang Y W, Yang G W, Huang C G. Influence of tunnel length on the pressure wave generated by high-speed trains passing each other. Sci China Tech Sci, 2012, 55: 255–263
9 Yonn T S, Lee S, wang J H, et al. Prediction and validation on the sonic boom by a high-speed train entering a tunnel. J Sound Vibr, 2001, 247: 195–211
10 Shin C H, Park W G. Numerical study of flow characteristics of the high speed train entering into a tunnel. Mech Res Commun, 2003, 30: 287–296
11 Yakhot V, Orszag S A. Renormalization group analysis of turbulence: I. Basic theory. J Sci Comput, 1986, 1: 1–51
12 Fluent Inc. FLUENT 6.3 User's Guide [EB/OL]. http://www.fluent.com
13 Mei Y G, Zhao Z H, Xu J L. High-speed Railway Tunnel Aerodynamics (in Chinese). Beijing: Science Press, 2009. 206–208
14 Pierre P, Arturo B, Paolo M. Nature of pressure waves induced by a high-speed train travelling through a tunnel. J Wind Eng Ind Aerodyn, 2007, 95: 781–808